Dynamic effects in transition from regular to Mach reflection in steady supersonic flows

Rohtash Goyal [*], A. Sameen [†], T. Jayachandran [‡] and G. Rajesh [§]
Department of Aerospace Engineering, Indian Institute of Technology Madras, Chennai 600036, India

The effect of rapid wedge rotation on the transition from regular (RR) to Mach reflection (MR) is investigated. This unsteady shock reflection transition is compared with the steady-state transition. The dependence of various flow features such as the unsteady Mach stem height, position of the reflection point, and shock angle at the reflection or triple point on the wedge angle for a fixed Mach number is compared at various rotation rates. The study is further extended to compare the dynamic effects for various Mach numbers in the strong shock reflection domain at higher wedge speeds. Transition lines corresponding to different rotation speeds are obtained similar to the detachment transition line in steady cases. It is found that the pivot point has only marginal effect on the transition point, but it substantially affects the Mach stem growth and the movement of the reflection point, specifically at higher Mach numbers. The location of the transition from the inlet also depends on the pivot point and the rate of rotation.

I. INTRODUCTION

Shock wave reflection is one of the interesting and important phenomena in high-speed flows. Shock wave reflections are observed in nozzle flows, supersonic inlets, and various other applications and are broadly classified into regular reflection (RR) and irregular reflection (IR) [1]. The most common type of irregular reflection observed in steady flows is a simple Mach reflection (SMR), also known as a Mach reflection (MR). There are clear, distinct features for RR and MR, best described with the help of a schematic diagram, as shown in Figs. 1(a) and 1(b). Regular reflection is a two-shock structure in which an incident shock wave (*i*) and a reflected shock wave (*r*) meet at the reflection point *R* as shown in Fig. 1(a). In the RR, the reflected shock wave induces an equal and opposite flow deflection to the one induced by the incident shock wave [2,3]. On the other hand, an MR is a three shock structure, consisting of an incident shock wave, a reflected shock wave, and a Mach stem (*m*) with a slipstream (*s*), intersecting at the triple point *T* as shown in Fig. 1(b). In the MR, the net flow deflection near the triple point induced by the incident and the reflected shock wave is equal to the flow deflection induced by the Mach stem [2,3]. The slipstream acts as a contact surface, and the pressure across it near the triple point is uniform. Apart from the standard solution of an IR, which is the MR, various nonstandard solutions such as von Neumann reflection (vNR) [4,5], Guderely reflection (GR) [6,7], and Vaislev reflection (VR) [8] which are collectively known as weak-Mach reflections (WMR) [9] exist and are not so common in steady flows.

These shock structures transit into one another depending on various parameters, a phenomenon known as shock wave transition [10]. The shock wave transitions commonly occurring in the steady flows are regular to Mach reflection (henceforth indicated as RR → MR) and Mach to regular reflection (MR → RR). It is important to identify the transition point because the transition leads to a significant change in the flow properties [11]. Azevedo and Liu [12] showed the significant influence of the subsonic region behind the Mach stem in acoustic pressure levels after the transition to MR, which could have been otherwise supersonic in an RR. Hence, the identification of the transition point in physical and parameter spaces is important in designing supersonic vehicles and engine inlets.

The steady-state RR ↔ MR transition has been a continued interest since the pioneering work of von Neumann [2]. A detachment condition for the transition RR → MR and the von Neumann condition for the transition MR → RR were introduced by von Neumann [2,3]. These criteria were not in complete agreement with the experimental results obtained for a wide range of Mach numbers and wedge angles [13]. The transition criteria also depend on the domain where the reflections happen. The shock reflections were classified into two domains [14], a weak shock reflection domain and a strong shock reflection domain based on a critical free stream Mach numbers $M_{0C} = 2.47$ for monoatomic gas and $M_{0C} = 2.2$ for diatomic gas. The flow downstream of the reflected shock is subsonic in a weak shock reflection domain, whereas it is supersonic in a strong shock reflection domain. A length scale criterion for RR → MR transition was also proposed, and it was postulated that, for a finite length scale (a Mach stem) to exist in an MR, there must be a communication of pressure signals to the reflection point through the expansion fan, which can only happen when the flow downstream of the reflection point is sonic, also known as the sonic criterion for RR → MR transition [15]. There have been several studies to

---

*ae18s007@smail.iitm.ac.in
†Corresponding author: sameen@ae.iitm.ac.in
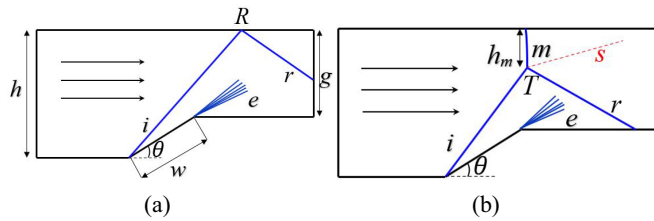‡t_jayachandran@iitm.ac.in
§rajesh@ae.iitm.ac.in

FIG. 1. Schematic representations of (a) regular reflection, (b) Mach reflection. Incident shock, i meets reflected shock r at point R in regular reflection and at point T in Mach reflection. Additionally, at T, Mach reflection has a third shock wave m, which is the Mach stem.

estimate the Mach stem height and overall MR configuration in both symmetric [11,16–19] and asymmetric [20–22] wedge reflections in steady flows, as the flow properties vary remarkably across the Mach stem.

It was first hypothesized that the transitions RR → MR and MR → RR could occur at different wedge angles [15], a phenomenon known as hysteresis in the wedge angle variation induced RR ↔ MR transition. There were failures in observing the hysteresis phenomenon because of its sensitivity to perturbations. Henderson and Lozzi [23,24] failed to record the hysteresis in their experiments and concluded that both RR ↔ MR transitions happen at the von Neumann condition. Hornung and Robinson [25] conducted experiments for various Mach numbers and concluded that strong disturbances and/or turbulence in the flow set up an information path and cause an early transition to MR at the von Neumann condition, and hence failed to observe the hysteresis. They also showed that the RR ↔ MR transition depends on whether the free stream Mach number M is more or less than a critical value M_{0C} given by [14]. The hysteresis in experiments was first demonstrated using extremely minimal noise levels in the wind tunnel to avoid any effect of perturbations on the transition point [26,27]. Hysteresis in the computational simulations was observed first by Chpoun *et al.* [28], followed by many others [29–34].

A review of the well-established steady-state RR ↔ MR transition criteria for the strong and weak shock reflections by Ben-Dor [10] discusses several applications. Both RR ↔ MR transitions occur at the steady detachment condition in the weak shock reflection domain. In contrast, a dual solution domain exists in the strong shock reflection domain, and the transition RR → MR occurs at the steady detachment condition while the transition MR → RR occurs at the von Neumann condition.

Although there are several studies available on the steady-state RR ↔ MR transition, limited reports exist on the unsteady shock reflection. The unsteadiness here is the rapid variation of wedge angle for a steady oncoming supersonic flow. The dynamic effects can be significant in practical applications involving rapidly flapping surfaces such as in supersonic inlets with wedge angle changing in time, thrust vectoring, and supersonic flow over control surfaces. One such investigation to study the maximum permissible rotation speed without introducing the dynamic effects was carried out by Khotyanovsky *et al.* [35]. They observed a shock curvature at higher speeds of wedge rotation. Mouton and Hornung [17] showed in their experiments that at a higher wedge rotation rate RR → MR transition is delayed, and RR can be maintained further into the dual solution domain but not up to or beyond the detachment condition. Felthun and Skews [36] did a computational investigation on the effects of rapid wedge rotation for constant Mach number $M = 3.0$. They observed that at higher wedge speeds RR → MR transition happens beyond the detachment condition, and MR → RR transition happens below the von Neumann condition.

Naidoo and Skews [37] provided the first experimental confirmation of RR → MR transition beyond the steady detachment condition in symmetric wedge reflection at higher wedge speeds. They conducted an experimental and computational study to investigate RR → MR transition criteria and the mechanism of the transition at rapid wedge rotation in the strong and weak reflection domain. It was found that the RR was maintained even in the presence of the length-scale information in the strong reflection domain (at $M = 2.98$), and the transition happened even before the appearance of the length-scale information in the weak reflection domain (at $M = 1.93$). Based on this, they concluded that the transition to MR in the dynamic case happens when the flow at the reflection point cannot be turned parallel to the wall by the reflected shock wave, which was termed the dynamic counterpart for the steady detachment condition. A brief parametric study was also done to investigate the effect of change in the point of rotation and the initial incidence on RR → MR transition. Naidoo and Skews [38] further extended this study to a wider range of rotation rates to confirm the RR → MR transition criteria in the dynamic case. They confirmed that the sonic, detachment, and length-scale criteria are different in the rapid wedge rotation, and the transition in the dynamic case occurs due to the inability of the flow to maintain the wall boundary conditions. Naidoo and Skews [39] studied the effect of rotation rate on the Mach stem growth in MR → RR transition. The sensitivity of the transition point to the pivot point and the initial incidence was also examined briefly. However, its influence on the Mach stem growth and the location of the transition from the domain inlet has not been studied. Their investigation was mainly focused on the RR → MR transition mechanism at higher wedge speeds. The previous studies involving dynamic effects were mostly done for a single Mach number $M = 2.98$ in the strong reflection domain. The present study aims to bridge these gaps, specifically to comare the dynamic effects at a wide range of rotation rates, Mach number, and pivot points, focusing on the specific flow features as mentioned above for symmetric shock reflection.

In the above studies, though the overall features of the dynamic shock transition phenomenon were presented, the dependence of flow features, such as the unsteady Mach stem height, position of the reflection point, and shock angle at the reflection point, on the wedge angle in the dynamic shock reflection regime for RR → MR transition were not discussed in detail. The influence of the above parameters on the aerodynamic forces generated on bodies traveling at supersonic speeds is significant. For example, the inlet cowl opening of a supersonic vehicle may generate dynamic effects depending on the speed at which it opens. The growth rate of the Mach stem after the RR → MR transition determines

how the unsteady pressure and temperature loads evolve on the geometry. The steady-state transition criteria may not predict the transitions and configuration of the Mach reflections, which are influenced significantly by the dynamic effect. The present study identifies the importance of dynamic effects in the shock reflection process.

We carried out a computational study of the dynamic RR → MR transition with the wedge angle changing in time. The methodology to simulate such continuously moving domains is discussed briefly. The important flow features investigated in the present work are the unsteady Mach stem height, position of the reflection or triple point, and shock angle at the reflection or triple point. A comparative analysis is done between the steady-state RR → MR transition and the transition at higher wedge speeds in the range $M_e \in [0.001, 0.1]$ for various Mach numbers in the range $M \in [2.5, 4.5]$. The wedge is rotated about different pivot points and the influence of the pivot point on the RR → MR transition and on some of the flow features is discussed.

II. NUMERICAL METHOD

The dynamic effects in RR → MR due to the wedge rotation involves moving surfaces in the computational domain. The grid and domain size are time dependent and hence the setup is computationally challenging. The shock reflection phenomenon is primarily inviscid in nature [10], and here we do not discuss the viscous effects. In this paper, the flow is simulated by solving two-dimensional (2D) compressible Euler equations for a time-dependent computational mesh and domain [40].

For a stationary control volume, the unsteady, compressible governing equations in the conservative finite volume form are given as

$$\frac{\partial \mathbf{q}}{\partial t} + \nabla \cdot \mathbf{F} = 0. \tag{1}$$

where, the vector $\mathbf{q}$ is the conserved quantity given as $\mathbf{q} = [\rho, \rho u, \rho v, \rho E]^T$, and $\mathbf{F}$ represents the convective flux vector of conserved variables. The local grid changes its volume and surface area as the domain changes in time. To account for the volume changes due to the local control surface velocity, the convective flux vector undergoes the transformation given as $\mathbf{F}^* = \mathbf{F} - \mathbf{q}\mathbf{W}$, where $\mathbf{W} = W_x \hat{i} + W_y \hat{j}$ is the local control volume face speed [40]. The velocity in the x and y directions for each face of the control volume is calculated based on the average of the velocities of the bounding nodes of that face; for example, the face from bounding nodes $n1$ and $n2$ is given by

$$W_x = \frac{\left(\frac{dx}{dt}\right)_{n1} + \left(\frac{dx}{dt}\right)_{n2}}{2}, \quad W_y = \frac{\left(\frac{dy}{dt}\right)_{n1} + \left(\frac{dy}{dt}\right)_{n2}}{2}. \tag{2}$$

Here, dx/dt and dy/dt are the velocities of the node in the x and y directions, respectively. Similarly W_x and W_y are evaluated for all four faces of the quadrilateral cell. For a moving control volume, $\mathbf{F}^*$ can then be written as [40]

$$\mathbf{F}^* = \begin{bmatrix} \rho(u - W_x) \\ \rho u(u - W_x) + p \\ \rho v(u - W_x) \\ (\rho E + p)(u - W_x) + W_x p \end{bmatrix} \hat{i} + \begin{bmatrix} \rho(v - W_y) \\ \rho u(v - W_y) \\ \rho v(v - W_y) + p \\ (\rho E + p)(v - W_y) + W_y p \end{bmatrix} \hat{j}. \tag{3}$$

The velocity of each node in the x and y directions is calculated based on the change in the position of that node in a time interval δt as

$$\frac{dx}{dt} = \frac{x_f - x_i}{\delta t}, \quad \frac{dy}{dt} = \frac{y_f - y_i}{\delta t}, \tag{4}$$

where the subscripts i and f represent initial and final nodal positions, respectively. The initial and final position of every node in δt time are known *a priori*, as the mesh movement is done with a predefined speed of wedge rotation. Each node is assumed to be moving at a uniform speed in the x and y directions. The nodal coordinates in the x and y directions are updated at each time step. The change of geometrical parameters such as surface area, volume, and normal vectors are also updated at each time step for all the elements.

The governing equations are solved using the cell-centered finite volume method on an unstructured quadrilateral mesh [41]. Convective flux across the interface is calculated using a second-order AUSM$^+$-up scheme formulated by Liou [42]. The gradients at the cell centers are calculated using the least-squares method, and values of the flow variables to the left and the right of the cell interfaces are computed using a Taylor series expansion with second-order accuracy along with the Venkatakrishnan limiter [43] to avoid the oscillations in the second-order accurate solution. For each face of the quadrilateral element, $\mathbf{F}^*$ given in Eq. (3) is computed using the values of the flow variables either to the left or the right of the cell interface, depending on the wave information travel, as discussed in [42]. The net flux vector $\mathbf{F}^*$ through each element is thus calculated by the summation of the flux through all the bounding faces of the element. A fourth-order Runge-Kutta scheme is used for time marching. The solver is optimized for speed using OPENMP.

A. Computational domain

The computational model in Fig. 2 shows the domain boundaries. Only one-half of the domain of symmetrical double wedge configuration is simulated by modeling the top boundary as a reflection plane. The velocity normal to the reflection plane is zero, and the normal gradient of all other primitive variables such as pressure, temperature, and density are also zero. The flow at the inlet is supersonic with $P_0 = 474k$ Pa and $T_0 = 302$ K, values consistent with the experiments for validation [37]. The outlet flow is supersonic, and all variables at the outlet are extrapolated from the domain.
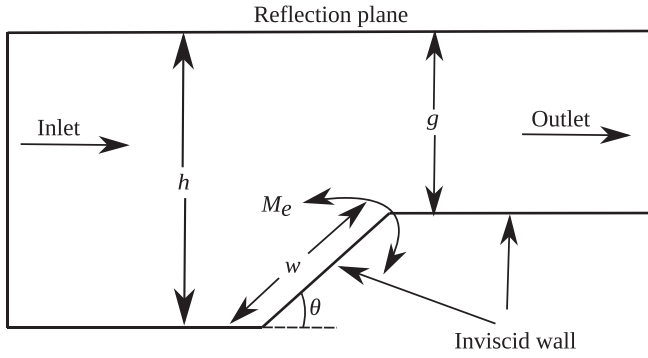
FIG. 2. Schematic diagram of the computational model. The wedge of length w is rotated at a fixed rotation rate M_e. In the figure, trailing edge pivot rotation is indicated. The wedge angle θ is measured from the horizontal as shown.

All the solid surfaces are modeled as slip walls, with the fluid having a tangential velocity relative to the wall while the normal velocity is zero. Similar to Felthun and Skews [36], a dimensionless rotation speed,

$$M_e = \frac{V_e}{a_\infty} = \frac{\Omega w}{a_\infty}, \tag{5}$$

is specified, which quantifies the moving edge speed (V_e) of the wedge in terms of free stream speed of sound (a_∞). Here, $V_e = \Omega w$ where Ω is the rate of wedge rotation, and w is the wedge length. The ratio g/w is fixed for the trailing edge pivot and h/w for the leading edge pivot.

The wedge is started from an initial angle and is rotated about the pivot points at a uniform speed to a final wedge angle. The initial and final nodal positions are obtained from the mesh at the initial and final wedge angles, respectively. The wedge is rotated about the trailing edge for most of the simulations unless otherwise specified and is compared with the flow features resulting from the leading edge pivot in some cases. The study is done for various values of $M_e \in [0.001, 0.1]$ and $M \in [2.5, 4.5]$. The time interval δt, during which the mesh moves from initial to final position, is computed based on M_e. The value of M_e for increasing wedge angle (anticlockwise rotation) is taken as positive, and that for decreasing wedge angle (clockwise rotation) is taken as negative. The initial condition for each case is the steady state solution attained for that particular initial wedge angle. The steady state solution for the initial wedge angle is obtained first before the wedge is continuously rotated to a final wedge angle.

B. Grid sensitivity

The study in this paper is carried out for various inlet Mach numbers M at various M_e, in the strong reflection domain ($M > 2.2$ for $\gamma = 1.4$). The prediction of the RR $\rightarrow$ MR transition is often considered a good marker for grid sensitivity [37,44]. The grid dependence of the solution is checked on the Mach number and M_e independently. Although a grid-independent solution is obtained on a coarser grid for lower Mach numbers, the same grid is found to be not suitable for higher Mach numbers. A comparatively finer grid is required for higher Mach numbers at the same M_e. Similarly, a finer grid is required for a grid-independent solution at a higher M_e

TABLE I. Variation of wedge angle at transition, θ_T, and shock angle at transition, ϕ_T (in degrees) with refinement as dimensionless minimum size of the element in the grid, s/w in RR $\rightarrow$ MR transition for $M = 4.5$ and $M_e = 0.1$. The grid system with $s/w = 0.0012$ is chosen as the final grid.

Number of elements	s/w	θ_T	ϕ_T
175 000	0.0048	32.4	42.9
350 000	0.0024	31.6	41.3
700 000	0.0012	31.2	40.5
1 000 000	0.00086	31.1	40.5
1 400 000	0.0006	31.1	40.4

for the same M. Thus, the grid sensitivity study is done for the "worst-case scenario" of this study, the highest Mach number ($M = 4.5$) and the highest rate of rotation, $M_e = 0.1$.

The wedge is rotated continuously for an incoming steady flow. Each simulation starts from an initial wedge angle θ_i and is rotated at a constant rate M_e. The results are recorded for every $0.1°$ of wedge rotation. The transition RR $\rightarrow$ MR is identified by the appearance of the Mach stem from the contour plots. The transition point is assumed to be at the instance at which the Mach stem appears first, in steps of $0.1°$ of the wedge rotation. A smaller Mach stem might not be captured by a coarser grid system, leading to a delayed transition point. The transition points for RR $\rightarrow$ MR are checked on various grids from coarser to finer until a grid-independent solution is obtained. The simulations start with a steady RR established at an initial wedge angle $\theta_i = 24°$ in the dual solution domain at $M = 4.5$, and the wedge is rotated at $M_e = 0.1$ until the transition occurs. The variation of the wedge angle at transition (θ_T) and shock angle at transition (ϕ_T) for different grids is shown in Table I. Also shown in Table I is the refinement of each grid in terms of the dimensionless minimum size of the element in the grid (s/w), where s is the minimum element size.

The shock angle (ϕ) is measured at the reflection point in an RR and at the triple point in an MR due to shock curvature in dynamic cases [35,36]. The angles were measured from the numerical schlieren. Lines passing through centers of these shocks are considered, as the shocks waves have a finite thickness, and the reflection and the triple points are identified at their intersections. A smaller value of s/w results in a higher Mach stem resolution and an early transition to MR than the coarser grids, as shown in Table I. The grid convergence is obtained as shown in Table I, and a grid system with $s/w = 0.0012$ is chosen as the final grid. The results shown in this paper henceforth are all for the grid with 7×10^5 quadrilateral elements with the refinement of $s/w = 0.0012$.

C. Validation of the code

Steady reflection RR $\rightarrow$ MR. The code is tested for various rotation rates, and it is confirmed that $M_e = 0.001$ is small enough for the flow to exhibit nearly steady-state behavior at each time step. A hysteresis test is done for the steady state for $M = 4.5$. For RR $\rightarrow$ MR, a steady RR is first established at an initial wedge angle $\theta_i = 24°$, as shown in Fig. 3(a), and
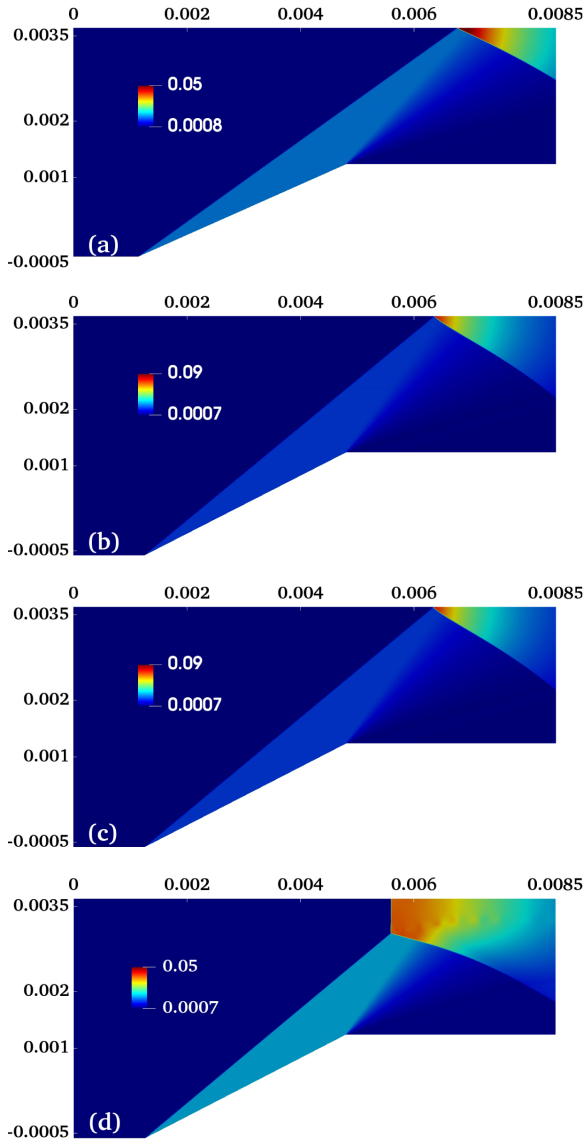
FIG. 3. The wedge rotation speed of $M_e = 0.001$ is found to be nearly steady shock reflection case for all M. The dimensions shown are in meters. Static pressure (in MPa) contours for $M = 4.5$ in steady RR → MR transition starts at (a) $\theta = 24.0°$ with a steady state solution and progressively increasing the wedge angle. The contours shown are just before the transition (b) $\theta = 27.0°$, at transition point (c) $\theta = 27.1°$, and just after transition (d) $\theta = 27.2°$. See Supplemental Material [45].
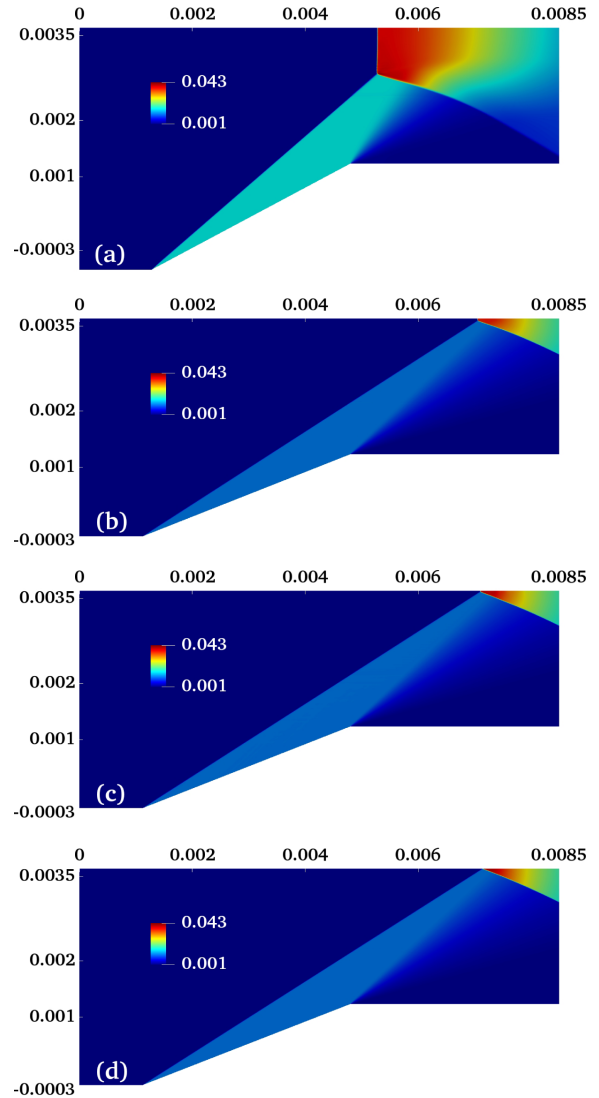

FIG. 4. The wedge rotation speed of $M_e = -0.001$ is nearly steady shock reflection case and the negative sign indicates decreasing wedge angle. The dimensions shown are in meters. Static pressure (in MPa) contours for $M = 4.5$ in steady MR → RR transition start at (a) $\theta = 28.0°$ with a steady state solution and progressively decreasing the wedge angle. Contours shown are just before transition (b) $\theta = 21.4°$, at transition (c) $\theta = 21.3°$, and after transition (d) $\theta = 21.2°$. See Supplemental Material [45].

the wedge angle is increased steadily at $M_e = 0.001$ until the transition to MR takes place. The transition is observed at a wedge angle, $\theta = 27.1°$, as shown in Fig. 3(c); the corresponding theoretical detachment criteria [10] is $\theta = 26.9°$. The pressure contours just before and after the transition are shown in Figs. 3(b) and 3(d), respectively. The comparison of shock angle is 39.4° against a theoretical value of 39.2° [10].

Steady reflection MR → RR. To validate the MR → RR transition at $M = 4.5$, the simulation starts from an MR case at $\theta_i = 28°$ and progressively decreases the wedge angle indicated by negative rotation speed. For MR → RR, a steady MR is first established at an initial wedge angle $\theta_i = 28°$, as shown

in Fig. 4(a) and the wedge angle is decreased steadily at $M_e = -0.001$, until the transition to RR occurs. The transition is observed at $\theta = 21.3°$ when the Mach stem size goes to zero, as shown in Fig. 4(c); the corresponding theoretical von Neumann criterion [10] is $\theta = 21°$. The pressure contours near the transition are shown in Figs. 4(b) and 4(d), respectively. The shock angle computed is 32.2°, whereas the theoretical value is 31.9° [10] for steady reflection MR → RR. The values of wedge angle and shock angle at transition are in good agreement with the theoretical values for both RR → RR and MR → RR.

Dynamic shock reflection. The code is validated with the results of dynamic wedge rotation about the trailing edge pivot ($g \approx 0.6w$) reported by Naidoo [46]. The Mach stem growth
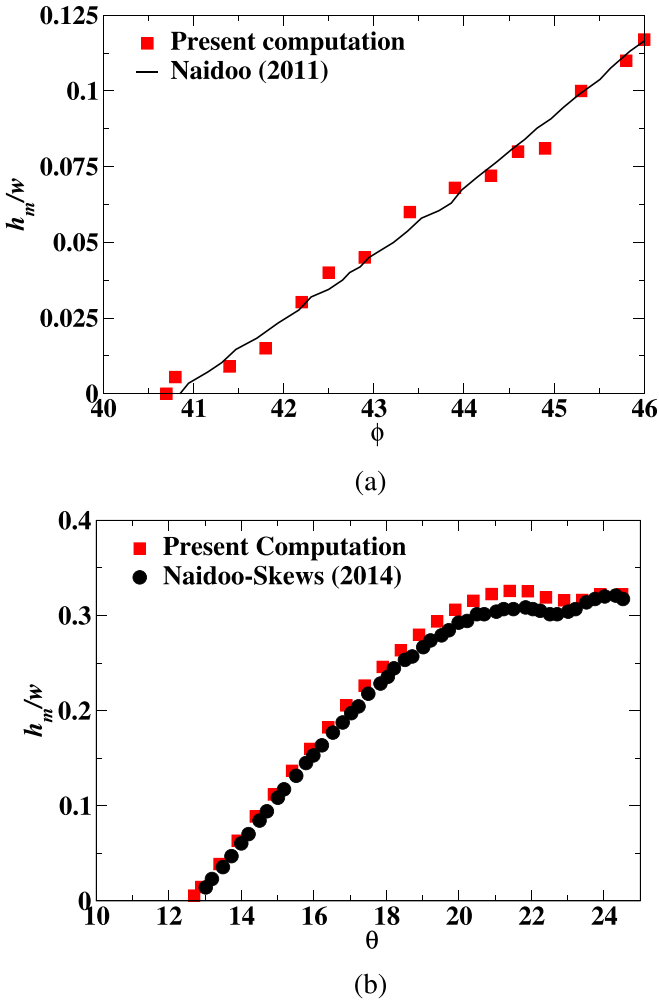
(a)

(b)

FIG. 5. Growth of the Mach stem for $M = 2.98$ with (a) shock angle in RR $\rightarrow$ MR due to the impulsive rotation of the wedge about the trailing edge at $M_e = 0.1$, and (b) wedge angle in MR $\rightarrow$ RR transition due to the impulsive rotation of the wedge about the trailing edge at $M_e = -0.05$.

FIG. 6. Growth of the Mach stem with wedge angle in RR $\rightarrow$ MR transition at various wedge rotation rates for $M = 4.5$.

III. STEADY AND DYNAMIC RR $\rightarrow$ MR TRANSITION

Felthun and Skews [36] briefly discussed the dynamic effects in RR $\rightarrow$ MR transition and reported a delay in transition at higher rates of wedge rotation. Naidoo and Skews [37] confirmed the delay in transition experimentally and mainly focused on the investigation of the criteria and mechanism of RR $\rightarrow$ MR transition at higher wedge speeds. Although Naidoo and Skews [37] compared the Mach stem growth with the shock angle for the steady and unsteady cases, the dependences of Mach stem height and various flow features such as the position of the reflection or triple point and the shock angle at the reflection or triple point on the wedge angle have not been compared at various M_e. They briefly investigated the effect of the pivot point on RR $\rightarrow$ MR transition; however, its influence on the Mach stem growth has not been studied. In this section, the dependences of various flow features such as the unsteady Mach stem height, the position of the reflection point, and shock angle at reflection or triple point on the wedge angle at various M_e for $M = 4.5$ are compared. The influence of the pivot point on RR $\rightarrow$ MR transition and the Mach stem growth is also investigated in detail.

A. Mach stem growth in rapid wedge rotation

The growth of the Mach stem (h_m/w) with the wedge angle and the shock angle at the triple point at various rates of rotation in RR $\rightarrow$ MR transition for $M = 4.5$ is investigated and compared. A steady RR is established at first for $M = 4.5$ at an initial wedge angle $\theta_i = 24°$. The wedge is started at the same $\theta_i = 24°$ for both the trailing and leading edge pivots to avoid the effect of initial incidence, if any, on the transition point, and the wedge angle is increased continuously at constant rates of rotation. At $\theta_i = 24°$, exit height g/w is 0.6 for rotation about the trailing edge and inlet height h/w is 1.0 for rotation about the leading edge (refer to Fig. 2).

In Fig. 6, the Mach stem height h_m/w is plotted against the wedge angle at various rotation speeds. Both cases of rotation, namely the leading and trailing edge pivots, are shown in the figure. After the transition point, there is a remarkable difference in the growth rate of the Mach stem for all M_e. The Mach

rate in RR $\rightarrow$ MR transition is the quantity that is used for comparison. A steady RR is established at first for $M = 2.98$ at an initial wedge angle $\theta_i = 19°$, and the wedge angle is increased from $\theta_i = 19°$ at a rotation rate of $M_e = 0.1$ until an MR is obtained. The variation of dimensionless Mach stem height (h_m/w), where h_m is the Mach stem height, is plotted against the shock angle (ϕ), and along with results from the 2D simulations of Naidoo [46] in Fig. 5(a).

Further, the dynamic MR $\rightarrow$ RR transition is compared with a test case from Naidoo and Skews [39]. As discussed in the previous case, a steady MR is first established for $M = 2.98$ at $\theta_i = 24.5°$ and wedge angle is progressively decreased at $M_e = -0.05$ until a RR is obtained. The Mach stem height is computed for all wedge angles as shown in Fig. 5(b), and the plot matches well with the literature.

In the next section, the influence of wedge rotation on various shock reflection parameters and indicators is analyzed for a wide range of M and M_e.
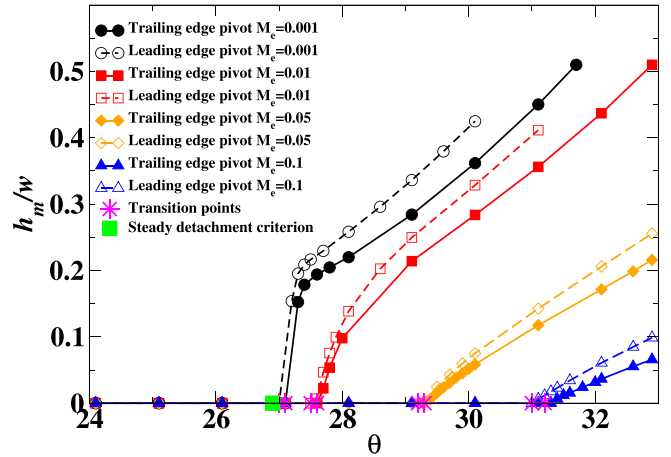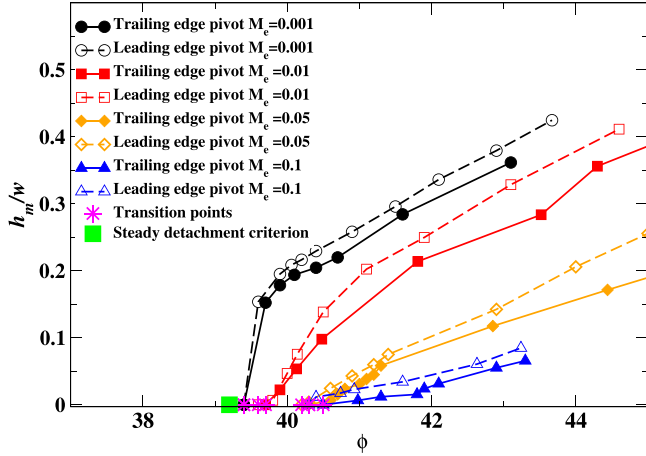
FIG. 7. Growth of Mach stem with shock angle at the triple point in RR $\rightarrow$ MR transition at various wedge rotation rates for $M = 4.5$.

FIG. 8. Dependence of the position of the reflection or triple point on the wedge angle in RR $\rightarrow$ MR transition at various rotation rates for $M = 4.5$.

stem after the transition point is smaller at higher M_e than at lower M_e. The Mach stem growth rate is abrupt closer to the transition point for the nearly steady case of $M_e = 0.001$ and decreases away from the point of transition. This can be seen from Fig. 6 by comparing the slope of the curves closer to the point of transition and away from it for $M_e = 0.001$. The slope shows an inflection point at lower M_e. On the other hand, at higher M_e, the Mach stem grows gradually after the transition. The Mach stem growth is found to be dependent on the pivot point and is higher for the leading edge pivot in comparison to the trailing edge pivot at a particular M_e for $M = 4.5$. Unlike the steady case, the transition happens beyond the detachment condition (shown as a green filled square) at higher θ on increasing M_e, which agrees with Felthun and Skews [36] and Naidoo and Skews [37].

In Fig. 7, the Mach stem height is plotted against the shock angle at the triple point at various rotation speeds for rotation about the leading and trailing edge pivots. The Mach stem growth with shock angle at the triple point at various M_e exhibits a similar trend as its variation with the wedge angle at various M_e. The Mach stem height for a particular shock angle is the highest for lower M_e, consistent with the observation of Naidoo [46] for $M = 2.98$. This can be attributed to the curvature of the incident shock in the dynamic case. It can be seen that the effective shock angle at the reflection point is less due to this curvature. This, in effect, corresponds to a lower wedge angle, causing a reduction in the size of the Mach stem. Apart from this, the growth of the Mach stem is qualitatively similar for all the rotation rates. A maximum difference of 0.2° is observed between the transition points of the trailing and leading edge pivots, which may be considered marginal. The delay in the wedge angle at transition is more than the shock angle at the transition from their corresponding steady-state values. Therefore, the influence of M_e on θ_T is higher as compared to ϕ_T, as can be understood from the fundamental θ-ϕ-M relations.

It should be noted from Fig. 7 that, although the transition points are nearly the same for both the pivots, the Mach stem height is affected by the location of the pivot point. The difference in the Mach stem size for the leading and trailing
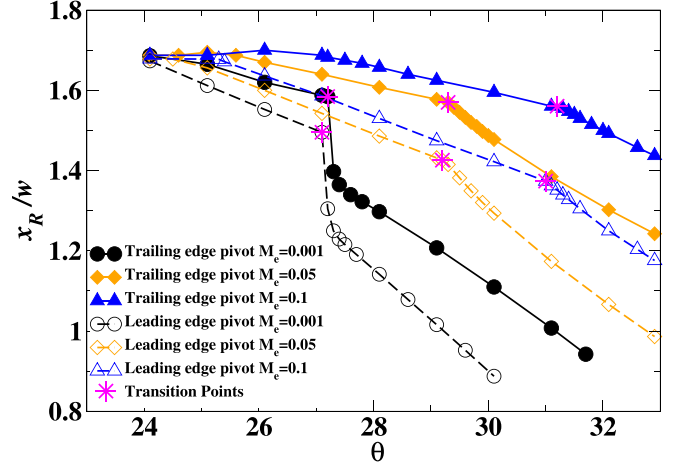
edge pivots becomes significant at higher shock angles. It is known that Mach stem height is a length scale in the flow field which depends on the geometry as well as the flow parameters such as the free stream conditions, inlet height, wedge length, and wedge angle. When the rotation is about the leading edge, the trailing edge height g changes, which may not have a direct influence on the Mach stem size, other than the effect of the wedge angle. On the other hand, when the rotation is about the trailing edge, the inlet height h changes, leading to a change in the Mach stem height.

B. Movement of the reflection or triple point in rapid wedge rotation

The variation of the position of the reflection or triple point (x_R/w) with the wedge angle is studied at various rates of rotation for RR $\rightarrow$ MR transition. Here, x_R is the distance of the reflection or triple point from the inlet of the domain. The influence of M_e on the location of the transition from the inlet and the dependence of the position of reflection or triple point on the pivot point is also investigated.

Figure 8 shows the dependence of reflection or triple point on wedge angle at various M_e for the rotation about the leading and trailing edge pivots. It can be seen from Fig. 8 that the reflection point starts moving immediately towards the inlet without any delay on increasing the wedge angle for $M_e = 0.001$ whereas, at higher M_e, the position of the reflection point is unchanged for some time when the wedge angle is increased. The delay in the movement of the reflection point increases as M_e increases, as seen for $M_e = 0.05$ and $M_e = 0.1$ in Fig. 8. This is because the flow in the steady wedge rotation has sufficient time available to set up a communication path for the information about the wedge rotation to get propagated to the reflection point. This results in the immediate movement of the reflection point in the steady case. However, at higher M_e, a lag in the communication of information occurs due to the finite speed of the disturbances carrying information about the wedge rotation. Hence, the
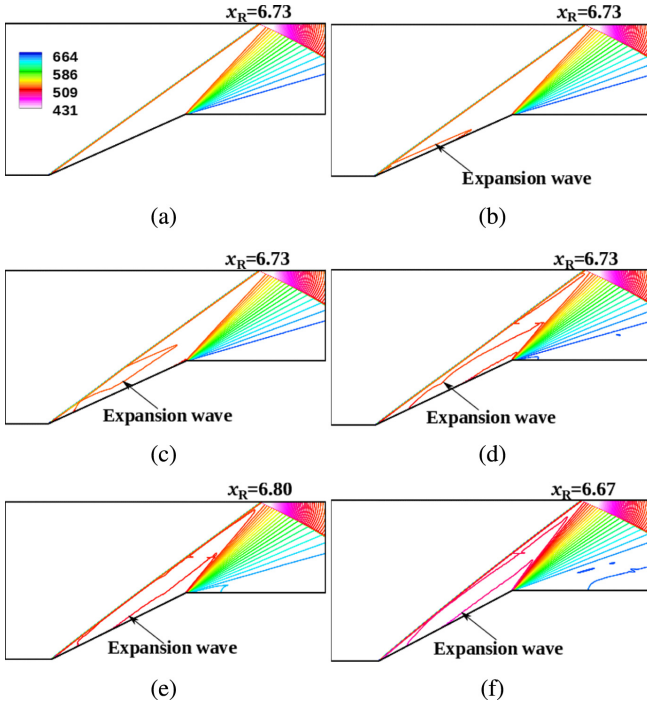
FIG. 9. Static pressure contours coloured with streamwise velocity u (m/s), for rotation about the trailing edge for $M = 4.5$, $M_e = 0.1$. The reflection point is indicated as x_R (mm) from the inlet; other dimensions are similar to those in Fig. 3. Rotation starts with a steady case at (a) $\theta_i = 24°$, and the x_R remains the same for (b) $\theta = 24.1°$; an expansion wave emanates from leading edge. Expansion waves continue to propagate and x_R remains stationary, (c) $\theta = 24.5°$, till expansion waves reach the reflection point at (d) $\theta_{cr} = 25.3°$. After θ_{cr}, the x_R starts moving towards the exit till it reaches (e) $\theta_m = 26.2°$. For any further increase in θ, the reflection point moves towards the inlet as in (f), $\theta = 27.8°$. See Supplemental Material [45].

wedge rotates by a significant amount at higher M_e before the reflection point starts moving.

The speed at which the reflection point moves towards the inlet changes after the flow undergoes the transition for all the rotation rates simulated in this study. This is evident from the change in gradient of the curves at the transition point, as shown in Fig. 8. A similar change in the gradient was observed in the unsteady experiments conducted by Naidoo and Skews [37]. From the present simulation, it is noted here that, at lower M_e, there is an abrupt change in gradient at the transition point due to the sudden appearance of the Mach stem. The change in the gradient is smaller on increasing M_e.

The speed of the motion of the reflection point is dependent on the pivot point and is higher for the leading edge pivot. The transition happens closer to the domain inlet for the leading edge pivot compared to the trailing edge pivot for a particular M_e. The difference in the location of transitions for both the pivots increases with M_e. Also seen from Fig. 8, the transition location is closer towards the inlet for higher M_e, more evidently for the leading edge pivot. Hence, the location of transition is found to be dependent on both the pivot point and M_e.

There are clear differences observed in the flow field depending on the choice of the pivot point. Figure 9 shows the

TABLE II. Effect of M_e on the movement of the reflection point for trailing edge pivot. Here, θ_{cr} is the wedge angle at which the expansion waves reach the reflection point, and θ_m is the wedge angle at which the reflection point starts moving towards the inlet.

M_e	0.01	0.05	0.1
θ_{cr} (degrees)	24.1	24.6	25.3
θ_m (degrees)	24.2	25.2	26.2

pressure contours for the rotation about the trailing edge at $M_e = 0.1$ for $M = 4.5$. As before, a steady RR is established first at $\theta_i = 24°$, as shown in Fig. 9(a). As the wedge angle is increased with a rotation rate of $M_e = 0.1$ about the trailing edge pivot, the expansion waves start emerging from the wedge surface because the leading edge moves away from the reflection plane [Fig. 9(b)]. These waves are seen at higher M_e, particularly at $M_e = 0.05$ and at $M_e = 0.1$, but are not present in the nearly steady case ($M_e = 0.001$). This is clearly a dynamic effect as visualized from the contour plots. Naidoo and Skews [39] have discussed the presence of similar waves and their effect on the Mach stem growth in MR $\rightarrow$ RR transition for rapid wedge rotation. The waves propagate towards the reflection point as shown in Fig. 9(c) and take a finite time to reach the reflection point.

Further, the wave propagation and reflection point affect each other as follows. In the supersonic flow, when the wedge is rotated about the trailing edge, the reflection point is unaware of the wedge movement. The position of the reflection point is unchanged until the waves emanating from the leading edge reach the reflection point, which happens at a critical wedge angle (θ_{cr}), which in this case is $\theta_{cr} = 25.3°$ [Fig. 9(d)]. The shock angle at the reflection point is also unchanged till θ_{cr}. As the wedge angle is increased beyond θ_{cr}, there is a slight but noticeable movement of the reflection point away from the domain inlet till a particular wedge angle (θ_m, here $\theta_m = 26.2°$), as in Fig. 9(e). On increasing the wedge angle beyond θ_m, the reflection point starts to move continuously towards the domain inlet [Fig. 9(f)]. The initial movement of the reflection point away from the inlet on increasing the wedge angle is contrary to its expected movement towards the inlet. This is because, for the trailing edge pivot, when the wedge angle is increased rapidly, the inlet height (h) increases at a constant shock angle at the reflection point. Because the position of the reflection point depends on the h and the shock angle, the reflection point moves slightly away from the inlet before it starts continuously moving towards the inlet at higher wedge speeds. Comparatively, at higher M_e, the reflection point moves farther away from the inlet before continuously moving towards it. On the other hand, for the steady case, an immediate movement of the reflection point towards the domain inlet is observed on increasing the wedge angle, unlike in the dynamic case. Expansion waves are not seen in the steady case as the flow has sufficient time to communicate the wedge movement to the reflection point.

Table II shows the wedge angle at which the expansion waves reach the reflection point (θ_{cr}) and the wedge angle at which the reflection point starts moving towards the inlet (θ_m) at various M_e for $M = 4.5$. The initial wedge angle (θ_i) for all the cases shown in Table II is 24°. It can be seen that θ_{cr} and
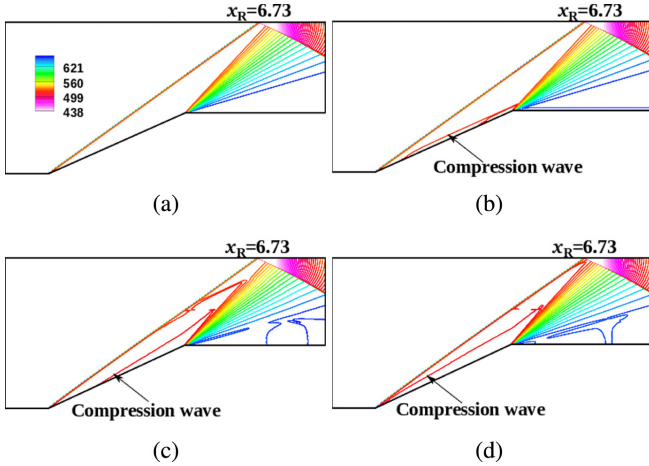
FIG. 10. Static pressure (in MPa) contours for rotation about the wedge leading edge for $M = 4.5$, $M_e = 0.1$. The reflection point is indicated as x_R (mm) from the inlet; the other dimensions are similar to those in Fig. 3. The simulation starts with a steady case at (a) $\theta_i = 24°$, and compression waves start emanating from the leading edge at (b) $\theta = 24.1°$. The reflection point is unaware of wedge movement even at (c) $\theta = 24.9°$, till the wave arrives at (d) $\theta_{cr} = 25.3°$. After θ_{cr}, the reflection point starts moving towards the inlet. See Supplemental Material [45].

θ_m are higher for higher M_e. This implies that the delay in the movement of the reflection point is higher for higher wedge speeds.

The dynamics wedge rotation about the leading edge produces almost similar flow features as the trailing edge pivot, except for the absence of a reflection point moving away from the inlet. Figure 10 shows the pressure contours for rotation about the leading edge at $M_e = 0.1$ for $M = 4.5$. A steady RR is established at $\theta_i = 24°$ for the leading edge pivot similar to the trailing edge pivot, as shown in Fig. 10(a). For rotation about the leading edge pivot, compression waves start emerging from the wedge surface as the trailing edge moves towards the reflection plane, as shown in Fig. 10(b). The waves travel towards the reflection point shown in Fig. 10(c). The reflection point is unaware of the wedge movement until these waves arrive at the reflection point at critical wedge angle (θ_{cr}, here $\theta_{cr} = 25.3°$) for $M_e = 0.1$ as shown in Fig. 10(d). On further increasing the wedge angle, the reflection point starts moving towards the domain inlet. As the inlet height h is constant for rotation about the leading edge, no movement of the reflection point away from the inlet is seen as in the case of the trailing edge pivot. The values of the critical wedge angle (θ_{cr}), at which the reflection point starts moving, is found to be nearly the same for both the pivots at a given M_e.

C. Shock angle at the reflection or triple point in rapid wedge rotation

In this section, the variation of the shock angle at the reflection or triple point with the wedge angle is examined. The variations of the wedge angle and the shock angle with time for various rotation rates are also discussed.
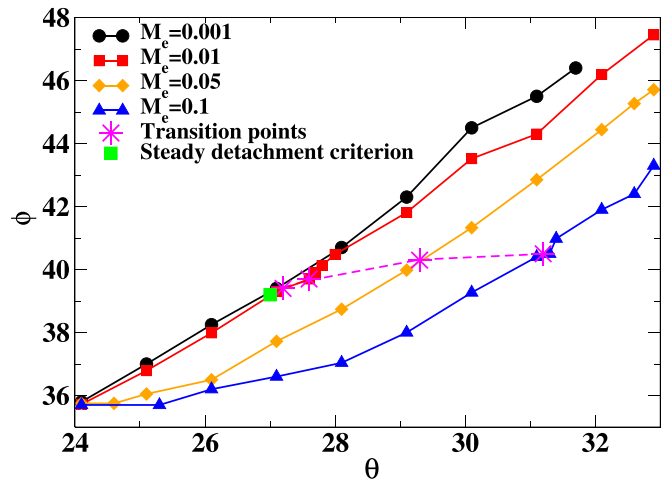

FIG. 11. Variation of the shock angle at the reflection or triple point with the wedge angle in RR → MR transition at various rotation rates for $M = 4.5$.

In Fig. 11, the shock angle is plotted with the wedge angle for various rotation speeds for rotation about the trailing edge pivot. For the steady case, ϕ increases on increasing θ. However, at higher M_e, the shock angle at the reflection point remains constant initially, as shown for $M_e = 0.1$ in Fig. 11, until the waves from the wedge surface reach the reflection point at θ_{cr}, after which it starts increasing. The change in slopes of the curves for dynamic cases in the figure suggests this regime change. For a particular wedge angle, ϕ at the reflection point is smaller at higher M_e. The shock angle at transition point ϕ_T is shown with the magenta star symbol (*) in Fig. 11. The value of ϕ_T is dependent on the shock curvature and increases with M_e. However, at higher M_e, the variation of ϕ_T seems to be asymptotic, a behavior previously noted by [36].

In Fig. 12(a), the wedge angle is plotted against the time for rotation about the trailing edge. The rotation rate is kept constant for the dynamic cases examined in this paper; therefore, the wedge angle increases linearly with time, as shown in the plot. The slope of the lines represents the magnitude of the rotation rate, M_e. The slope is the highest for $M_e = 0.1$ and least for $M_e = 0.001$. As seen from the plot, the transition (symbols magenta star) happens at higher θ but earlier in time at higher M_e. Figure 12(b) shows the variation of θ_T/ϕ_T with time for various rotation rates. It can be seen from the plot that θ_T increases more rapidly than ϕ_T on increasing the rotation rate. This is surmised as follows: the value of ϕ_T at the reflection or triple point in the dynamic case depends on the shock curvature, and, at a higher M_e, the wedge rotates by a higher amount but a comparatively lower variation in the curvature.

D. Transition lines for RR → MR

There are well-established transition criteria for steady RR → MR transition [10]. In steady cases, the wedge angle at which the transition occurs for a particular Mach number can be identified from the detachment line. In this section, transition lines for RR → MR transition over a range of Mach
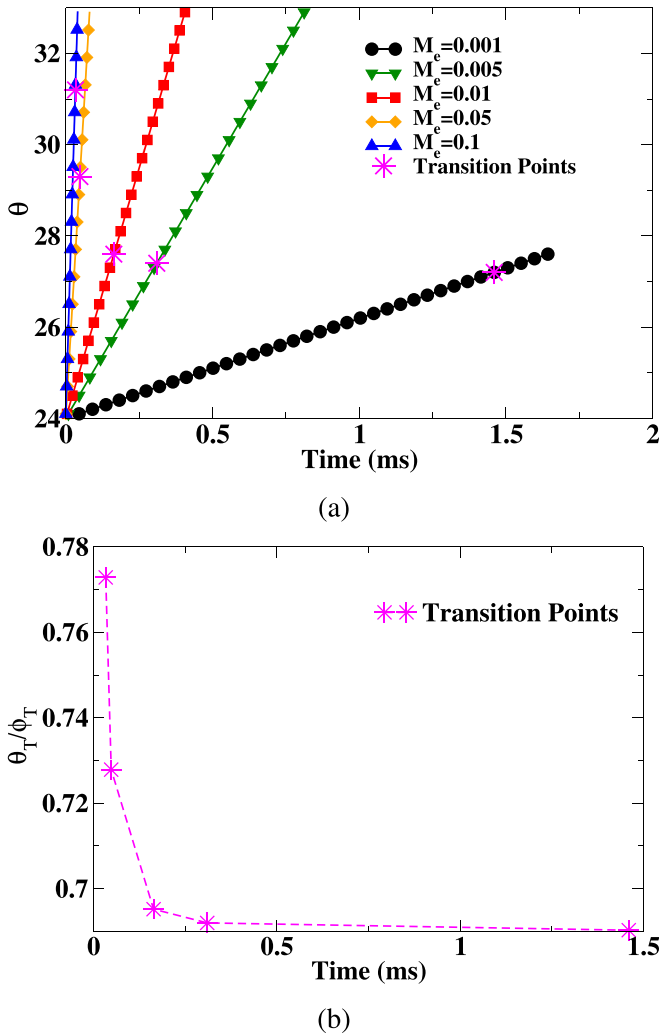
(a)

(b)

FIG. 12. Variation of (a) the wedge angle with time, (b) θ_T/ϕ_T with time, at various rotation rates for $M = 4.5$.
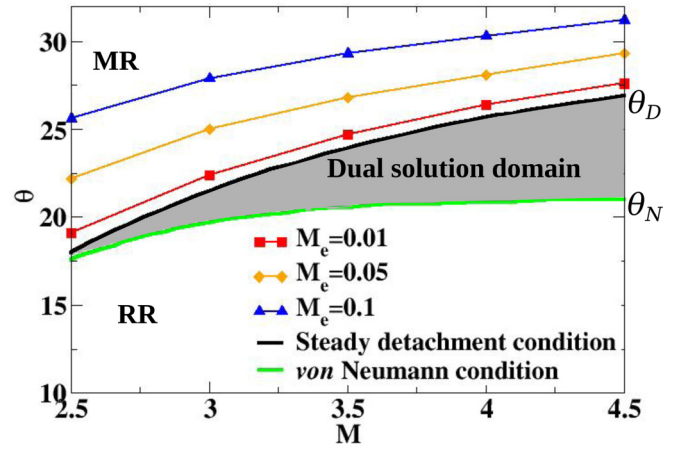

FIG. 13. The wedge angle at transition plotted against M for various M_e. The loci of these points are called the transition lines, here shown for RR $\rightarrow$ MR.

numbers, $M \in [2.5, 4.5]$ at $M_e \in [0.01, 0.1]$ in the dynamic case, are discussed. The investigation to study the influence of the initial wedge angle (θ_i) on the transition point for the dynamic case is also carried out.

As a range of Mach numbers is investigated, it is necessary to choose the correct range of wedge angles for each Mach number such that $H_{t\min} < H_t < H_{t\max}$ (where H_t represents the distance between the trailing edge and the reflection plane) given by Ben-Dor [10] to obtain stable RR and MR configurations. These initial wedge angles are chosen such that a stable RR configuration can be obtained for that particular Mach number. The initial wedge angles (in degrees) and the corresponding Mach numbers are the following pairs: $[M, \theta_i] = [(2.5, 17); (3.0, 20); (3.5, 22); (4.0, 24); (4.5, 24)]$.

The wedge angle is progressively increased from an initial wedge angle for each of the Mach numbers, as already discussed in the previous sections. Figure 13 shows the wedge angle plotted against M, for various M_e; the locus of these points is the transition lines. It can be observed from Fig. 13 that the wedge angle at transition is increasing with an increase in M_e for all M. At lower M, the difference between

steady detachment and transition point for a given M_e is higher than for a higher M.

The influence of initial wedge angle on transition points is investigated next. A steady RR is established for $M = 4.5$ at two different initial wedge angles, $\theta_i = 24°$ and $\theta_i = 18°$. The wedge angle is increased continuously from these initial states at various M_e until the transition to MR is attained. The wedge angle at transition (θ_T) and shock angle at transition (ϕ_T) are computed and tabulated in Table III. From the table, it can be seen that the transition happens at the same wedge angle and shock angle irrespective of the initial wedge angle, and the transition points are independent of the initial wedge incidence.

E. Effect of Mach number on Mach stem growth at higher wedge speeds

In this section, the nondimensionalized Mach stem height (h_m/h, where h_m is the Mach stem height and h is the distance between the leading edge and the reflection plane) variation with wedge angle is investigated. Here, h_m/h is plotted instead of h_m/w as in the earlier section because the wedge length w remains the same for all the runs in this section. Since the h value is different for each Mach number, plotting h_m/h leads to better comparison among the Mach stem growth rates for various Mach numbers.

Figures 14(a) and 14(b) show the development of the Mach stem with the wedge angle in RR $\rightarrow$ MR transition at $M_e =$

TABLE III. Effect of initial wedge angle θ_i on RR $\rightarrow$ MR transition at various M_e for $M = 4.5$. Transition points are independent of the initial wedge angle.

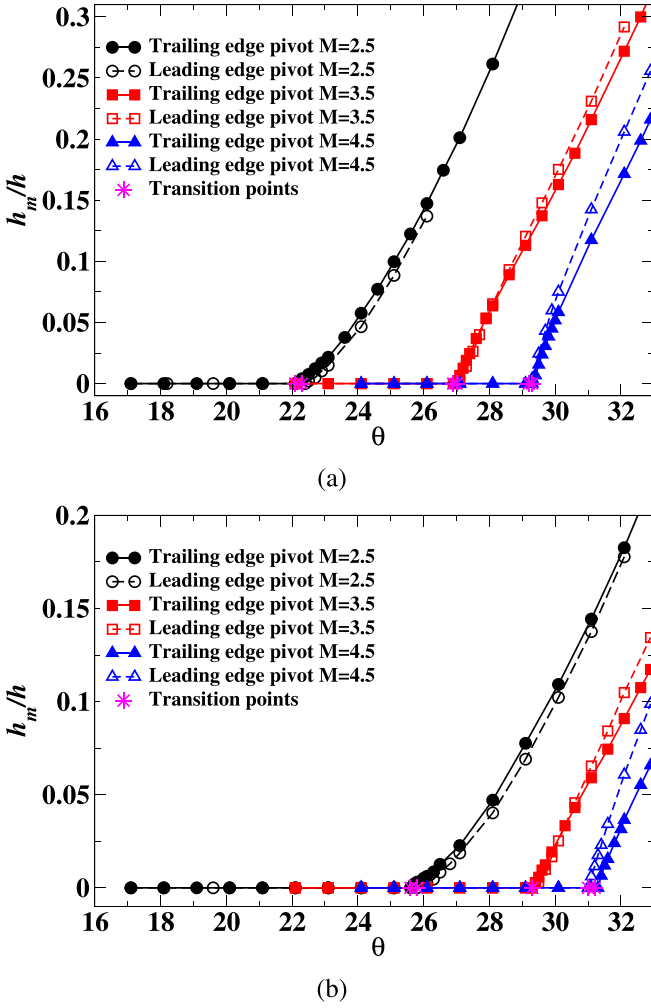| Transition	$\theta_i = 24°$		$\theta_i = 18°$	
	θ_T	ϕ_T	θ_T	ϕ_T
$M_e = 0.01$	27.6°	39.6°	27.6°	39.5°
$M_e = 0.05$	29.3°	40.2°	29.3°	40.3°
$M_e = 0.1$	31.2°	40.5°	31.2°	40.5°

(a)

(b)

FIG. 14. Development of the Mach stem along the wedge angle for various Mach numbers at (a) $M_e = 0.05$, (b) $M_e = 0.1$ in RR → MR transition.

0.05 and 0.1 respectively. In both these plots, Mach stem height at a particular wedge angle is higher for lower Mach number, which is similar to the Mach stem growth in steady wedge rotation. The slope of the lowest Mach number curve closer to the point of transition is comparatively smaller than the slope of the other two curves. This implies that, just after the transition point, the Mach stem growth rate is higher for higher Mach numbers. It is also observed from these plots that the difference in the Mach stem heights between the leading and trailing edge pivots is minimal at lower Mach numbers, while it is more prominent at higher Mach numbers (particularly at $M = 4.5$). Hence, the difference in the Mach stem growth between the leading and trailing edge pivots is dependent on the Mach number. However, the transition points are nearly the same for both the leading and trailing edge pivots for all the Mach numbers, as shown in Table IV.

F. Effect of Mach number on the movement of the reflection or triple point at higher wedge speeds

In Sec. III B, the effect of M_e on the position of the reflection or triple point for a fixed Mach number ($M = 4.5$) was

TABLE IV. Effect of the pivot point on the transition wedge angle in RR → MR transition for various Mach numbers.

M	2.5	3.5	4.5
Trailing edge pivot ($M_e = 0.01$)	19.1°	24.7°	27.6°
Leading edge pivot ($M_e = 0.01$)	19.1°	24.7°	27.5°
Trailing edge pivot ($M_e = 0.05$)	22.2°	26.8°	29.3°
Leading edge pivot ($M_e = 0.05$)	22.3°	27.0°	29.2°
Trailing edge pivot ($M_e = 0.1$)	25.6°	29.3°	31.2°
Leading edge pivot ($M_e = 0.1$)	25.8°	29.3°	31.0°

discussed. It was observed that the position of the reflection point at higher wedge speeds is unchanged until the compression or expansion waves generated from the wedge surface reach the reflection point at a critical wedge angle, θ_{cr}. In this section, the influence of the Mach number on the movement of the reflection or triple point is examined.

The movement of the reflection point is monitored with the wedge movement at a given rate of rotation for various Mach numbers. The angle ($\Delta\theta$, in degrees) by which the wedge rotates before the waves reach the reflection point is noted for each Mach number for various $M_e \in [0.01, 0.1]$ and is shown in Table V. It is clear from the table that the wedge rotates by a higher amount at the lower Mach numbers before the waves reach the reflection point, This means that the propagation speed of these waves decreases at lower Mach numbers, and hence the time taken to communicate the wedge movement to the reflection point is higher.

Figures 15(a) and 15(b) show the position of reflection point (x_R/w) with wedge angle for various Mach numbers at $M_e = 0.05$ and 0.1 respectively. As seen from these figures, the transition happens further away from the domain inlet on increasing the Mach number. The difference between the locations of transition is reduced on increasing Mach number. The reflection point moves faster in the leading edge pivot case for all the Mach numbers, and the change in the speed of the reflection or triple point at the transition is higher at higher Mach numbers.

The quantitative information deduced from this work consists of the Mach stem growth rate after the RR → MR transition and the estimation of the movement of the reflection point. The extent of the Mach stem height determines the area of the subsonic domain behind it. For an aerodynamic body, the information of the subsonic region is crucial since additional aerodynamic forces are generated on the supersonic body due to the RR → MR transition. The location and move-

TABLE V. Angle ($\Delta\theta$) by which the wedge rotates before the reflection point starts moving, for various Mach numbers at various rotation rates.

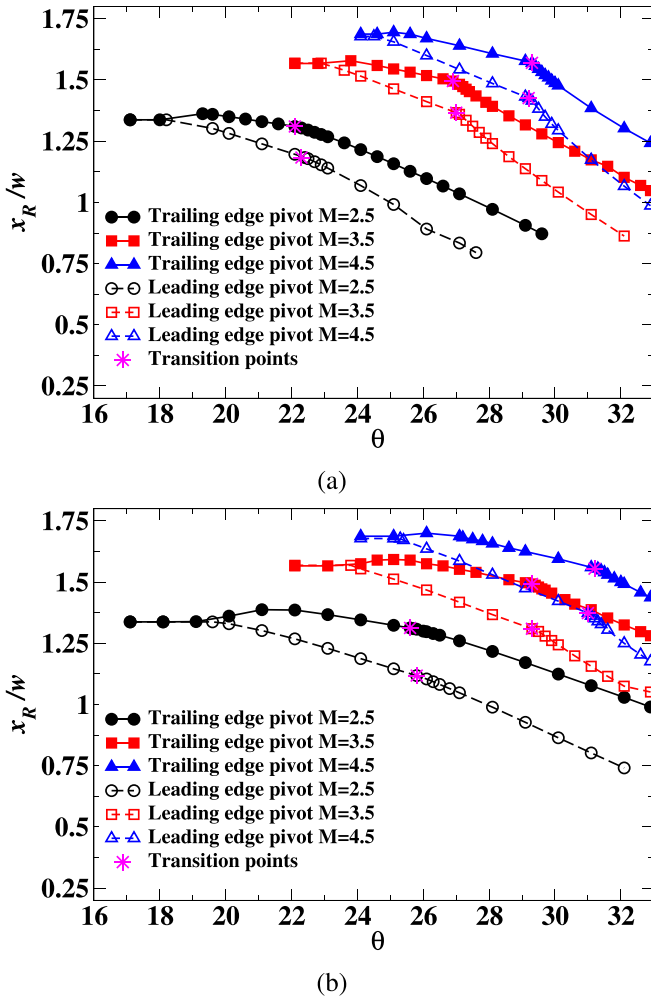| M_e	0.01	0.05	0.1
$M = 2.5$	0.2°	1.0°	2.6°
$M = 3.0$	0.2°	0.9°	2.1°
$M = 3.5$	0.1°	0.8°	1.8°
$M = 4.0$	0.1°	0.7°	1.4°
$M = 4.5$	0.1°	0.6°	1.3°

FIG. 15. Dependence of the position of the reflection or triple point for various Mach numbers at (a) $M_e = 0.05$, (b) $M_e = 0.1$ in RR $\rightarrow$ MR transition.

ment of the reflection point will help in estimating unsteady loads on the supersonic body.

IV. CONCLUSION

A computational study of the dynamic RR $\rightarrow$ MR transition with the wedge angle changing in time is carried out. The transition lines at various dynamic wedge speeds are obtained.

The RR $\rightarrow$ MR transition occurs at a higher wedge angle and a higher shock angle beyond the steady detachment angle at higher wedge speeds, consistent with the previous results [36,37]. The delay in the transition beyond the wedge angle at the steady detachment condition is higher for lower Mach numbers at a particular M_e. After the transition point, there is a remarkable difference in the growth rate of the Mach stem for various M_e. At the transition point, the Mach stem is smaller at higher M_e, and for the nearly steady case of $M_e = 0.001$ there is an abrupt change in the growth rate. The flow features such as the unsteady Mach stem height and the movement of the reflection point depend on the pivot point. The difference in the Mach stem heights between the leading and the trailing edge pivots is more significant at higher Mach numbers, with the leading edge pivot having a higher growth rate than the trailing edge pivot. For all the rotation speeds and the Mach numbers tested, in the rotation about the trailing edge, the reflection point moves slower than the rotation about the leading edge. The wedge rotates by a higher amount before the reflection point starts moving at higher wedge speeds and lower Mach numbers. The transition point for the leading edge pivot is closer to the inlet than the trailing edge pivot for all the cases tested, and the difference in the locations of the transition points increases as the wedge speeds increase. θ_T increases more rapidly than ϕ_T on increasing the rotation rate; however, the variation of ϕ_T seems to reach an asymptotic value at higher M_e.

The findings confirm that the dynamic effects such as the rate of wedge rotation cannot be neglected in wedge angle variation induced transition. The transition points itself are modified due the rapid wedge rotation. Another important aspect where the dynamic effects have a large influence is the development of the overall Mach reflection configuration. The rate of the wedge rotation in the dynamic case significantly alters the Mach reflection configuration from that of the steady cases. The characteristic changes in the MR configuration would help quantify the transient forces generated on supersonic bodies where RR $\rightarrow$ MR transition occurs due to the geometry changes. These will provide useful inputs to the supersonic or hypersonic vehicle designers.

ACKNOWLEDGMENT

[1] E. Mach, Uber den verlauf von funkenwellen in der ebene und im raume, Sitzungsbr. Akad. Wiss. Wien **78**, 819 (1878).

[2] J. von Neumann, *Oblique Reflection of Shocks*, Explosives Research Report 12 (Navy Department, Bureau of Ordinance, Washington, DC, 1943).

[3] J. von Neumann, *Refraction, Intersection and Reflection of Shock Waves*, NAVORD Report 203-45 (Navy Department, Bureau of Ordinance, Washington, DC, 1945).

[4] P. Colella and L. F. Henderson, The von Neumann paradox for the diffraction of weak shock waves, J. Fluid Mech. **213**, 71 (1990).

[5] B. W. Skews and J. T. Ashworth, The physical nature of weak shock wave reflection, J. Fluid Mech. **542**, 105 (2005).

[6] K. G. Guderley, *Considerations on the Structure of Mixed Subsonic-Supersonic Flow Patterns*, Technical Report F-TR-2168-ND (Headquarters Air Materiel Command, Wright Field, Dayton, OH, 1947).

[7] E. I. Vasilev, T. Elperin, and G. Ben-Dor, Analytical reconsideration of the von Neumann paradox in the reflection of a shock wave over a wedge, Phys. Fluids **20**, 046101 (2008).

[8] E. I. Vasilev, Four-wave scheme of weak Mach shock wave interaction under von Neumann paradox conditions, Fluid Dynamics **34**, 421 (1999).

[9] M. Olim and J. Dewey, A revised three-shock solution for the Mach reflection of weak shocks ($1.1 < M_i < 1.5$), Shock Waves **2**, 167 (1992).

[10] G. Ben-Dor, *Shock Wave Reflection Phenomena* (Springer, Berlin, 2007), Vol. 2.

[11] H. Li and G. Ben-Dor, A parametric study of Mach reflection in steady flows, J. Fluid Mech. **341**, 101 (1997).

[12] D. Azevedo and C. S. Liu, Engineering approach to the prediction of shock patterns in bounded high-speed flows, AIAA J. **31**, 83 (1993).

[13] G. Ben-Dor, M. Ivanov, E. Vasilev, and T. Elperin, Hysteresis processes in the regular reflection ↔ Mach reflection transition in steady flows, Prog. Aerospace Sci. **38**, 347 (2002).

[14] S. Mölder, Particular conditions for the termination of regular reflection of shock waves, CASI Trans. **25**, 44 (1979).

[15] H. G. Hornung, H. Oertel, and R. Sandeman, Transition to Mach reflexion of shock waves in steady and pseudosteady flow with and without relaxation, J. Fluid Mech. **90**, 541 (1979).

[16] D. Azevedo, Analytic prediction of shock patterns in a high-speed, wedge-bounded duct, Ph.D. thesis, State University of New York, 1989.

[17] C. A. Mouton and H. G. Hornung, Experiments on the mechanism of inducing transition between regular and Mach reflection, Phys. Fluids **20**, 126103 (2008).

[18] B. Gao and Z. Wu, A study of the flow structure for Mach reflection in steady supersonic flow, J. Fluid Mech. **656**, 29 (2010).

[19] C.-Y. Bai and Z.-N. Wu, Size and shape of shock waves and slipline for Mach reflection in steady flow, J. Fluid Mech. **818**, 116 (2017).

[20] S. Roy and G. Rajesh, Analytical prediction of Mach stem height for asymmetric wedge reflection in 2-D steady flows, in *International Symposium on Shock Waves* (Springer, Berlin, 2017), pp. 855–863.

[21] Y. Tao, W. Liu, X. Fan, B. Xiong, J. Yu, and M. Sun, A study of the asymmetric shock reflection configurations in steady flows, J. Fluid Mech. **825**, 1 (2017).

[22] S. Roy and R. Gopalapillai, An analytical model for asymmetric Mach reflection configuration in steady flows, J. Fluid Mech. **863**, 242 (2019).

[23] L. Henderson and A. Lozzi, Experiments on transition of Mach reflexion, J. Fluid Mech. **68**, 139 (1975).

[24] L. Henderson and A. Lozzi, Further experiments on transition to Mach reflexion, J. Fluid Mech. **94**, 541 (1979).

[25] H. G. Hornung and M. Robinson, Transition from regular to Mach reflection of shock waves Part 2. The steady-flow criterion, J. Fluid Mech. **123**, 155 (1982).

[26] A. Chpoun, D. Passerel, H. Li, and G. Ben-Dor, Reconsideration of oblique shock wave reflections in steady flows. Part 1. Experimental investigation, J. Fluid Mech. **301**, 19 (1995).

[27] M. Ivanov, A. Kudryavtsev, S. Nikiforov, D. Khotyanovsky, and A. Pavlov, Experiments on shock wave reflection transition and hysteresis in low-noise wind tunnel, Phys. Fluids **15**, 1807 (2003).

[28] A. Chpoun, D. Passerel, J.-C. Lengrand, H. Li, and G. Ben-Dor, Mise en évidence expérimentale et numérique d'un phénomène d'hystérésis lors de la transition réflexion de Mach-réflexion régulière, Comptes rendus de l'Académie des Sciences, Ser. IIb: Mec. Phys. Chim. Astron. **319**, 1447 (1994).

[29] A. Chpoun and G. Ben-Dor, Numerical confirmation of the hysteresis phenomenon in the regular to the Mach reflection transition in steady flows, Shock Waves **5**, 199 (1995).

[30] M. Ivanov, S. Gimelshein, and A. Beylich, Hysteresis effect in stationary reflection of shock waves, Phys. Fluids **7**, 685 (1995).

[31] M. Ivanov, D. Zeitoun, J. Vuillon, S. Gimelshein, and G. Markelov, Investigation of the hysteresis phenomena in steady shock reflection using kinetic and continuum methods, Shock Waves **5**, 341 (1996).

[32] G. Ben-Dor, T. Elperin, and E. Golshtein, Monte Carlo analysis of the hysteresis phenomenon in steady shock wave reflections, AIAA J. **35**, 1777 (1997).

[33] M. Ivanov, G. Markelov, A. Kudryavtsev, and S. Gimelshein, Numerical analysis of shock wave reflection transition in steady flows, AIAA J. **36**, 2079 (1998).

[34] Y.-C. Hu, W.-F. Zhou, Z.-G. Tang, Y.-G. Yang, and Z.-H. Qin, Mechanism of hysteresis in shock wave reflection, Phys. Rev. E **103**, 023103 (2021).

[35] D. Khotyanovsky, A. Kudryavtsev, and M. Ivanov, Numerical study of transition between steady regular and Mach reflection caused by free-stream perturbations, in *Proceedings of the 22nd International Symposium on Shock Waves* (University of Southampton, Southampton, 2000) pp. 1261–1266.

[36] L. T. Felthun and B. W. Skews, Dynamic shock wave reflection, AIAA J. **42**, 1633 (2004).

[37] K. Naidoo and B. W. Skews, Dynamic effects on the transition between two-dimensional regular and Mach reflection of shock waves in an ideal, steady supersonic free stream, J. Fluid Mech. **676**, 432 (2011).

[38] K. Naidoo and B. W. Skews, Consideration of the effect of length-scale information on regular to Mach reflection transition in the presence of dynamic effects, in *International Symposium on Shock Waves* (Springer, Berlin, 2013), pp. 1355–1360.

[39] K. Naidoo and B. W. Skews, Dynamic transition from Mach to regular reflection of shock waves in a steady flow, J. Fluid Mech. **750**, 385 (2014).

[40] R. Biedron, V. Vatsa, and H. Atkins, Simulation of unsteady flows using an unstructured navier-stokes solver on moving and stationary grids, in *23rd AIAA Applied Aerodynamics Conference* (AIAA, Reston, VA, 2005) p. 5093.

[41] J. Blazek, *Computational Fluid Dynamics: Principles and Applications* (Butterworth-Heinemann, London 2015).

[42] M. Liou, A sequel to AUSM, part II: AUSM+-up for all speeds, J. Comput. Phys. **214**, 137 (2006).

[43] V. Venkatakrishnan, Convergence to steady state solutions of the Euler equations on unstructured grids with limiters, J. Comput. Phys. **118**, 120 (1995).

[44] L. Laguarda, S. Hickel, F. Schrijer, and B. Van Oudheusden, Dynamics of unsteady asymmetric shock interactions, J. Fluid Mech. **888**, A18 (2020).

[45] See Supplemental Material at http://link.aps.org/supplemental/10.1103/PhysRevE.104.055101 for movies of relevant pressure contours.

[46] K. Naidoo, Dynamic shock wave reflection phenomena, Ph.D. thesis, University of the Witwatersrand, (2011).